Surface-stabilized ferroelectric liquid-crystal diffraction gratings with micrometer-scale pitches

Carl V. Brown and Emmanouil E. Kriezis

The first-order diffraction efficiency η_1 of surface-stabilized ferroelectric liquid-crystal (SSFLC) phase gratings is calculated for device thicknesses in the range $d = 1$ to 5 μm and for pitches p of 5 to 20 μm assuming incident light at 633 nm. The peak value of η_1 as a function of d has negligible dependence on the incoming polarization when $p = 20$ μm. For smaller pitch values the peak value of η_1 decreases and becomes increasingly dependent on the orientation of the incoming polarization owing to the influence of the domain walls that occur between the SSFLC pixels. © 2004 Optical Society of America

OCIS codes: 050.1950, 160.3710, 200.4650, 260.1180.

1. Introduction

Switchable or reconfigurable liquid-crystal (LC) diffraction gratings are important components for applications in which beam-steering and optical routing are required, such as in optical-fiber-based telecommunication systems and in many other optical computing systems.[1–5] Surface stabilized ferroelectric liquid-crystal (SSFLC) phase gratings have many desirable properties for these applications. They have fast switching speeds, useful for optical correlation systems, and they are bistable, which means that they can be used in optical memories or in display systems in which an image is built up from tiled sections over time.[6–9] However, for telecommunication applications the most important requirement is that the diffraction efficiency of the grating is independent of the incoming polarization. This independence is necessary for minimizing insertion losses, because the polarization of light emerging from a fiber is uncertain and, moreover, may also fluctuate over time.[10]

An idealized representation of a one-dimensional (1D) SSFLC phase grating is depicted in Fig. 1. This grating is a series of uniform birefringent wave plates in which the in-plane twist angle of the optical axis is at a fixed magnitude but alternates in sign between adjacent wave plates (or pixels). The electric field vector of the normally incident light is depicted by $\mathbf{E}_{\mathrm{IN}}$. If the optical states are at twist angles $+\beta$, giving output electric field $\mathbf{E}_1$, and $-\beta$, giving output electric field $\mathbf{E}_2$, then the fraction of the incident light intensity η that is diffracted out of the zero order by this phase grating is given by the following equation, independent of the plane of polarization of the incident light[11,12]:

$$\eta = \sin^2(\pi \Delta n d/\lambda)\sin^2(2\beta). \tag{1}$$

Here Δn is the difference in refractive indices parallel and perpendicular to the optical axis, d is the thickness of the ferroelectric LC (FLC) layer, and λ is the free-space wavelength of incident light. Equation (1) holds, provided that pixels are substantially larger compared with the optical wavelength. It is immediately clear from Eq. (1) that the maximum diffraction efficiency can be achieved if the birefringent layers conform to the half-wave plate condition $\Delta n d/\lambda = 0.5$ and the switching angles are given by $\beta = 45°$. To describe the fraction of the incident light η_1 that is diffracted only into the two first-order diffraction spots, it is necessary to multiply the right-hand side of Eq. (1) by the coefficient $(4/\pi^2)$.[13]

Equation (1) applies in the polarization-insensitive mode of operation in which the entrance and the exit polarizers are removed. Arbitrarily polarized light passing though a pixel experiences an alteration in its polarization state. Note that this is distinct from the pure phase modulation that would be expected for a polarizer that was aligned along the bisector of the

C. V. Brown (carl.brown@ntu.ac.uk) is with the School of Science, Division of Physics and Mathematical Sciences, The Nottingham Trent University, Nottingham NG11 8NS, United Kingdom. E. E. Kriezis is with the Department of Electrical and Computer Engineering, Aristotle University of Thessaloniki, Thessaloniki GR-54124, Greece.

Received 20 February 2004; revised manuscript received 14 May 2004; accepted 17 May 2004.

0003-6935/04/285287-08$15.00/0

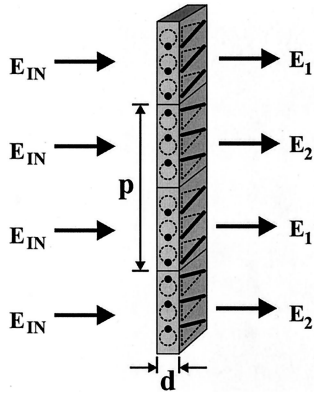

Fig. 1. Idealized 1D phase grating structure consisting of an array of birefringent plates. The in-plane twist angle of the optical axis of each plate has a fixed magnitude, but it alternates in the sign between adjacent wave plates.

two oppositely twisted pixel states. By averaging the polarization states $\mathbf{E}_1$ and $\mathbf{E}_2$ that emerge from pixels that are in opposite twist states, assuming equal number of pixels in the two possible states and subtracting the result from the incident intensity, it is possible to derive the equation.[11,12] Because of this averaging process the resulting expression is independent of the incoming polarization. However, this result only holds true provided (i) the pixel size is large enough to guarantee an independent treatment of each pixel state and (ii) it is possible to describe fully the optical effect of the LC layer with a simple 2×2 Jones matrix.

In reality, a phase grating utilizing FLC aligned in the SSFLC geometry will have an internal structure through the thickness of the layer, as schematically depicted in Fig. 2.[14,15] The SSFLC geometry is based on FLC materials that show an isotropic–nematic–smectic A–smectic C* phase sequence. The optical axis at a given depth within the layer is determined by the time-averaged direction of the LC molecules, i.e., the LC director. The director is tilted at an angle θ to the layer normal in the ferroelectric smectic C* phase. In addition, because of the combined effects of layer shrinkage and surface pinning during cooling into the smectic C* phase, the smectic layers tilt at an angle δ and form a chevron structure, as depicted in Fig. 2. In the C2U geometry, which is shown, the director lies parallel to the rubbing or easy alignment direction at each surface but twists out to one of two possible bistable positions on moving through the layer from the surfaces toward the chevron interface at the center of the cell. [The phrase C2U refers to a chevroned layer of type 2 with a uniform (i.e., untwisted) equilibrium director orientation.]

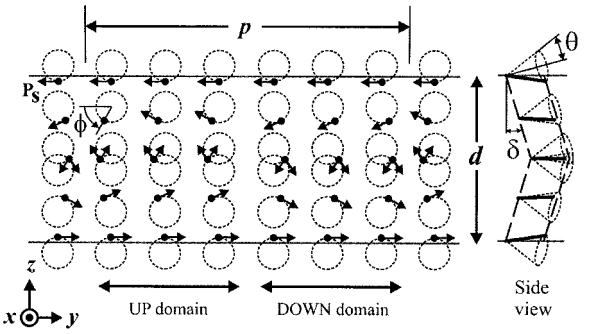

Fig. 2. Representation of the internal structure of a SSFLC diffraction grating. The position of the LC director at a point within the layer, shown by the filled circles, is defined by the azimuthal angle $\phi(y, z)$.

The effect of this internal director structure on the diffraction efficiency of an SSFLC phase grating was investigated in our previous publication.[16] The grating consisted of alternate up and down domains as depicted in Fig. 2. It was shown that the magnitude of the diffraction efficiency η_1 still does not depend on the polarization angle of the incident light. However, this result only holds true if (i) there are abrupt transitions from one type of domain to another, (ii) variations of the director orientation within each domain occur only in the z direction, i.e., through the thickness of the cell, and (iii) pixels are at a length scale substantially larger than the optical wavelength.

In fact, in a real SSFLC device the transition regions between adjacent domains of different types are not abrupt and a region of deformation in both the y and the z direction known as a domain wall occurs at these boundaries.[17] Reducing the pixel size and introducing the domain walls results in complicated wave components crossing the LC layer, which from a physical point of view cannot be correctly recast in the context of two simple Jones matrices. In the present study the influence of the two-dimensional (2D) director structure of a domain wall on the diffraction efficiency has been investigated. When the size of the pitch of the phase grating approaches the width of the SSFLC cell the additional variation in the director structure in the y as well as the z direction will be shown to have a significant effect on both the magnitude and the polarization dependence of η_1.

2. Theory

The geometry of a SSFLC phase grating with thickness d is depicted in Fig. 2. The orientation of the director at each position in the LC layer in the y–z plane is shown by a filled circle. The angle $\phi(y, z)$ gives the azimuthal rotation of the director around a cone of half angle θ. The arrows depict the direction of the spontaneous polarization vector, which has a constant magnitude $|\mathbf{P}(y, z)| = P_s$ and is fixed in relation to ϕ. Two switched states, up and down are shown, which correspond to the two bistable positions of the director at the chevron interface $\phi(y, d/2) = \phi_{ch}$ and $\phi(y, d/2) = \pi - \phi_{ch}$, where $\phi_{ch} = \arcsin(\tan \delta / \tan \theta)$. The twist angle is defined as the projection of the director orientation onto the x–y plane, measured with respect to the y axis. Therefore a twist angle of $\beta = 0$ rad corresponds to the azimuthal angles $\phi = \pm\pi/2$ rad. In the up domain the director twists from 0° at each surface (alignment direction) to

the maximum angle of $\beta = +\beta_{ch} = \arccos(\cos\theta/\cos\delta)$ at the chevron interface. In the down domain the maximum twist angle at the chevron interface is $\beta = -\beta_{ch}$.

The free energy that has been used to describe the 2D orientation of the LC director within the SSFLC diffraction grating is given in Eq. (2).[18]

$$2W = B\left[\left(\frac{\partial\phi}{\partial y}\right)^2 + \left(\frac{\partial\phi}{\partial z}\right)^2\right] - P_S\left(\sin\phi\,\frac{\partial V}{\partial y} + \cos\delta\,\cos\phi\,\frac{\partial V}{\partial z}\right). \quad (2)$$

The first term on the right-hand side is the elastic energy with an assumed isotropic smectic C elastic constant B. The second term arises from the electrostatic energy $\mathbf{P}\cdot\mathbf{E}$, where $\mathbf{E}$ is the electric field vector and, as usual, $\mathbf{E} = -\nabla V$, with V being the electrostatic potential. Solutions will be sought here only for the equilibrium structures that exist within the device when there is no externally applied field. To greatly simplify the 2D calculation, we used a single anisotropic dielectric permittivity ε_r for the FLC material. This single permittivity assumption is equivalent to neglecting the coupling between the biaxial dielectric anisotropies and the spontaneous polarization. The errors introduced into the calculation from making this assumption can readily be shown to be small for values of the spontaneous polarization and the three biaxial permittivities that are typical of commercial materials used in SSFLC devices.[19]

Equation (2) is minimized with the Euler–Lagrange equation in ϕ, $\partial\phi/\partial y$, and $\partial\phi/\partial z$. The resulting expression is discretized in terms of finite differences and is then solved with a forward Euler relaxation technique on a rectangular mesh. At the boundaries the values of ϕ were fixed at $\phi(y, 0) = +\pi/2$ and $\phi(y, d) = -\pi/2$ rad.

The potential profile was calculated simultaneously at all points on the mesh by use of the Maxwell's equation $\nabla\cdot\mathbf{D} = 0$. The displacement field vector is given by $\mathbf{D} = \varepsilon_O\boldsymbol{\varepsilon}\mathbf{E} + \mathbf{P}$. Equation (3) is given by the substitution of the dielectric permittivity ε_r, the electric field $\mathbf{E}$, and the polarization vector $\mathbf{P}$, with their explicit dependence on the azimuthal angle ϕ, into the Maxwell equation. This equation has been solved subject to the boundary conditions $V(y, 0) = V(y, d) = 0$.

$$0 = -\varepsilon_O\varepsilon_r\left(\frac{\partial^2 V}{\partial y^2} + \frac{\partial^2 V}{\partial z^2}\right) + P_S\left(\cos\phi\,\frac{\partial\phi}{\partial y} - \cos\delta\,\sin\phi\,\frac{\partial\phi}{\partial z}\right). \quad (3)$$

To avoid a divergence in the numerical solution occurring because of the discontinuity in the direction of the polarization vector at the chevron interface, $z = d/2$, it is necessary to re-express the Euler–Lagrange equation and Eq. (3) in an appropriate equivalent mathematical form.

Table 1. LC Material Parameters Used throughout the Simulations

Parameter	Numerical Value
Elastic constant B	5.7 pN
Spontaneous polarization P_S	6.5×10^{-5} C/m^2
Permittivity ε_r	5.09
Smectic cone angle θ	26.0°
Layer tilt angle δ	21.1°
Refractive index n_o	1.6317
Refractive index n_e	1.4789

One can calculate the optical tensor $[\varepsilon_{ij}]$ from the 2D director twist configuration found by solution of Eqs. (2) and (3) using the values of the uniaxial refractive indices (n_o, n_e) given in Table 1. The first-order diffraction efficiency η_1 is then calculated from this optical tensor by use of a rigorous vector beam-propagation method (VBPM) appropriate for LC devices.[20] This method provides a wide-angle forward-only numerical solution to Maxwell's equations and correctly incorporates the optical anisotropy effects presented by the inhomogeneous LC layer. Another alternative might have been the finite-difference time-domain method,[21,22] however, for this particular class of problems, almost identical results will have been obtained at the expense of much higher computational burden.

3. Diffraction Efficiency in the Long-Pitch Limit

One can investigate the diffraction efficiency of an SSFLC phase grating in the long-pitch limit by calculating variations in the director orientation, $\phi(z)$, in the z direction only. The twist profile derived from this calculation, $\beta(z)$, is then used in the up domain. The same profile, but with opposite polarity $-\beta(z)$, is used to describe the down domain. If an abrupt boundary is implemented between the up and the down domains, then the width of any deformation associated with the domain wall between the two regions is effectively zero.

The angles of the different diffracted orders are obviously determined by the pitch p. However, for light at normal incidence and as long as p is much larger than λ, the fraction of the incident light intensity that is diffracted to each of the diffraction orders will not depend on the exact choice of p, because there is no variation in the y direction within each domain and the domain walls have zero width. In terms of the first-order diffraction efficiency (η_1), this geometry will therefore be entirely equivalent to the limiting case for which the domain walls do have a nonzero width, but the value of the pitch p has become infinite.

Equilibrium 1D director profiles $\phi(z)$, allowing variations in the z direction only, have been calculated with the procedure outlined in Section 2 for a number of different cell thicknesses. Table 1 gives the values of elastic constant B, spontaneous polarization P_S, and permittivity ε_r that were used in the

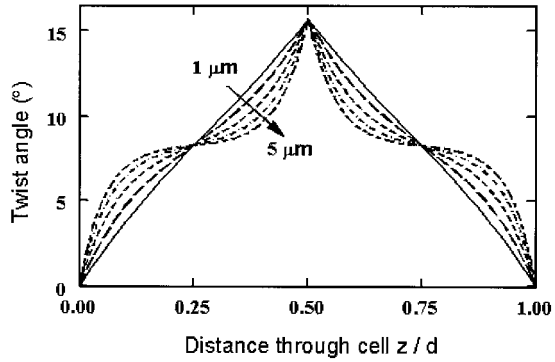

Fig. 3. Twist profiles (1D) showing the variation in the twist of the LC or director as a z section through the SSFLC layer depicted in Fig. 2. The increased influence of the magnitude of the spontaneous polarization on the twist profile is evident as the layer thickness is increased.

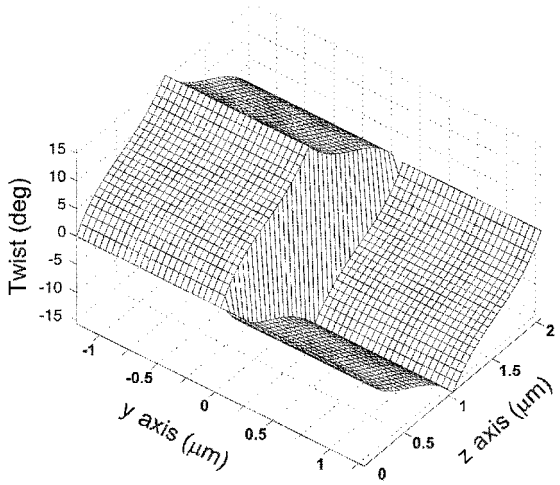

Fig. 4. Twist profile (2D) in the vicinity of a domain wall between up and down domains. This profile has been created by application of the 1D director twist profile for $d = 2$ μm in Fig. 3 to the geometry shown in Fig. 2 so that the transition region between the domains is abrupt.

calculations. The variation of the twist angle through the cell $\beta(z)$ for these profiles is shown in Fig. 3. These curves are derived from the profiles $\phi(z)$ and by use of simple trigonometrical formulas with the values for δ and θ given in Table 1. The values in Table 1 are based on reported measurements on the commercial FLC material SCE8*.[19]

For a cell thickness of $d = 1$ μm in Fig. 3 the twist profile varies approximately linearly between the surfaces and the chevron interface. This variation has been referred to in the literature as the twisted director profile (TDP).[15] This profile occurs when the elastic term in Eq. (2) is dominant over the P_s term. However, as the thickness is increased, the profiles in Fig. 3 become distorted away from the TDP as the self-interaction forces due to the spontaneous polarization become more dominant.[23] These forces oppose changes in the orientation of the polarization $\mathbf{P}$ and act to cause the LC director to align in a uniform orientation at one particular angle ϕ throughout the layer. The change in profile with thickness occurs because of the thickness dependencies of these two contributions to the free energy: the P_s self-interaction energy is approximately independent of the thickness d, whereas the elastic energy goes approximately as the reciprocal of d. Corresponding tilt profiles have also been obtained, and they are used in all subsequent optical calculations. However, as tilt angles are typically only few degrees, they are not shown for the brevity of space.

Figure 4 shows a 2D twist profile in the vicinity of a domain wall, which has been created from the 1D director twist profile for $d = 2$ μm in Fig. 3 applied to the geometry shown in Fig. 2. The up domain in the region $y < 0.0$ μm has a z variation of the twist corresponding to the 1D director twist profile for a cell thickness of 2 μm shown in Fig. 3. The down domain in the region where $y > 0.0$ μm has the same twist profile in the z direction with the opposite polarity. Within each domain no variation of the twist exists in the y direction, and there is an abrupt change from one twist direction to the other at the boundary between the two regions. Alternate up and down domains are repeated in the y direction with a period of 20 μm.

The first-order diffraction efficiency η_1 has been calculated for the profile in Fig. 4 using the VBPM with normally incident light at a wavelength of 632.8 nm that is linearly polarized in the y direction. The results for this profile and a range of other cell thicknesses are shown in Fig. 5 as a function of the dimensionless parameter $\Delta nd/\lambda$. Each value of $\Delta nd/\lambda$ represents a different LC layer thickness d and therefore, as illustrated by Fig. (3), a different director profile in the z direction. The optical anisotropy Δn and the wavelength λ have been kept constant such that the half-wave plate condition $\Delta nd/\lambda = 0.5$ occurs when the cell thickness is given by $d = 2$ μm. The lowest cell thickness used in the calculation was $d = 1$ μm. The curve has been smoothly extrapolated to the origin in the region $\Delta nd/\lambda < 0.25$. This approach is more rigorous than that described in our

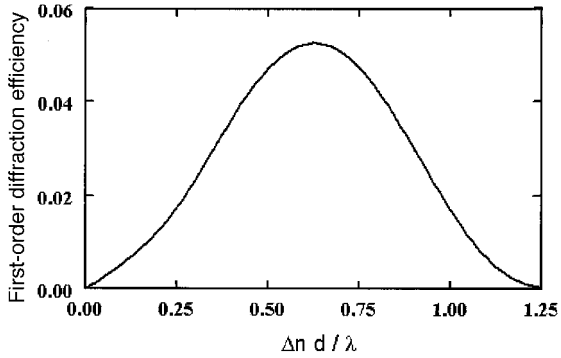

Fig. 5. First-order diffraction efficiency in the long-pitch limit η_1 as a function of the parameter $\Delta nd/\lambda$ for the diffraction geometry shown in Fig. 2. Profiles such as that shown in Fig. 4 were used in the calculations.

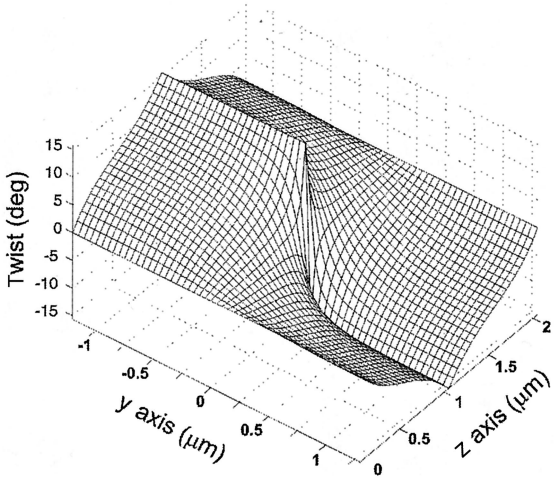

Fig. 6. Twist profile (2D) in the vicinity of a domain wall between up and down domains. Equations (2) and (3) were used to calculate this profile directly for a layer thickness of $d = 2$ μm.

previous publication in which the same director profile was used for each plot of η_1 versus $\Delta nd/\lambda$.[16]

The peak in the diffraction efficiency lies at $\Delta nd/\lambda = 0.63$. This peak is above the half-wave plate condition $\Delta nd/\lambda = 0.5$ that would be expected for an array of infinitely long uniform birefringent slabs. However, it is below the value of $\Delta nd/\lambda = 0.75$ that was found in our previous research for an array of TDPs of alternating polarity.[16] This result is consistent with the observation in Fig. 3 that the twist profile is close to a TDP for a small layer thickness, $d \sim 1$ μm but becomes increasingly uniform as the cell thickness increases to $d = 5$ μm and above. The peak in η_1 therefore occurs between the peak values expected for a completely uniform profile (i.e., a birefringent slab) and those expected for a TDP.

The curve shown in Fig. 5 is exactly the same whether the incident light is polarized in the x or the y direction, or at any orientation in between. This polarization insensitivity of the diffraction efficiency holds true in the long-pitch limit for the general case of an array of phase plates with twist profiles that alternate in polarity between $\beta(z)$ and $-\beta(z)$.[24–26]

4. Diffraction Efficiency with Small Pixels

The diffraction efficiency of SSFLC phase gratings will now be investigated for the case in which the full 2D director profile $\phi(y, z)$ is calculated by solution of Eqs. (2) and (3), allowing variations in ϕ in both the y and the z directions and using the LC parameters that are given in Table 1. At the chevron interface the values of ϕ are fixed at either $\phi(y, z = d/2) = \pm\phi_{ch}$ for the up domains or $\phi(y, z = d/2) = \pm(\pi - \phi_{ch})$ for the down domains, taking the positive sign when approaching the boundary from above and the negative sign when approaching from below.

Figure 6 shows a 2D twist profile $\beta(y, z)$ in the vicinity of the boundary wall between up and down domains of a linear SSFLC phase grating structure. Once again this has been converted from a $\phi(y, z)$ profile by use of simple trigonometrical formulas with the values for δ and θ given in Table 1. The cell thickness is 2 μm, and the grating pitch is 20 μm. The boundary between the up and the down domains in this figure occurs at $y = 0.0$ μm, where there is an abrupt change in the twist angle at the chevron interface $z = d/2$. In addition, the corresponding tilt profiles have been obtained but are not shown.

In the regions between the chevron interface and the surface, the twist profile, which has been determined by solution of Eqs. (2) and (3), changes more smoothly between the up and the down domains. The rate of change of the twist angle between the two domains in these regions is determined in part by the magnitude of the elastic constant B. A larger value of B would mean that changes in twist angle cost more elastic energy; so the rate of change of twist would reduce, leading to a larger region of elastic deformation at the domain boundary. Conversely, a smaller value of the elastic constant would mean that the elastic deformation was more localized to the boundary region. The change in twist angle as a function of distance z through the layer in the regions away from the boundary, i.e., near to $y = -1.25$ and $y = +1.25$ μm, is similar to the profiles shown in Fig. 3. This change indicates that the influence of the boundary distortion has been significantly diminished at this distance.

The curves shown in Figs. 7(a) and 7(b) illustrate the variation of the twist through a domain wall between an up and a down domain. The variation of the twist angle is shown as a function of distance in the y direction at $z = d/4$, where the total width of the region shown in the y direction is 2.5 μm. The boundary between the up and the down domain occurs at $y = 0.0$ μm in the center of each figure. Results are shown for layer thicknesses between $d = 1$ μm and $d = 5$ μm for two different phase grating pitches: $p = 5$ μm [Fig. 7(a)] and $p = 20$ μm [Fig. 7(b)]. The curve for $d = 2$ μm in Fig. 7(b) is therefore a section through the profile shown in Fig. 6.

A general observation from Fig. 7 is that the gradient at the boundary, i.e., the rate of change of twist with distance in the y direction in the center of the figures, decreases as the cell thickness increases. This decrease means that the width of the region of elastic distortion associated with the domain boundary increases with d. This behavior is expected for an elastic energy of the Laplacian form in Eq. (2).[27] Comparison of results for the two grating pitches, $p = 5$ μm [Fig. 7(a)] and $p = 20$ μm [Fig. 7(b)], shows that the gradient of the twist at the boundary is very similar for a given cell thickness.

The main differences between Figs. 7(a) and 7(b) occur in the regions away from the boundary. Since the width of each figure corresponds to 2.5 μm in the y direction, this corresponds to half the pitch length for the case $p = 5$ μm. Thus in Fig. 7(a) the points at the edges of the graph, $y = \pm 1.25$ μm, are exactly between and are equidistant from two domain boundaries. As the cell thickness is increased, the twist angle at $y = \pm 1.25$ μm decreases because of the

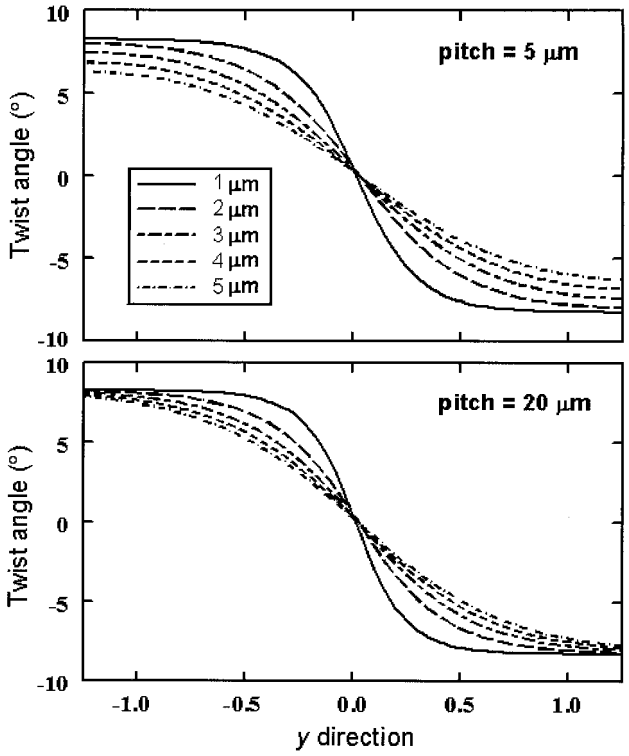

Fig. 7. Variation of the twist through a domain wall between an up and a down domain. The twist angle is shown as a function of distance in the y direction at $z = d/4$, where the total width of the region shown in the y direction is 2.5 μm and the domain wall is at the center of each figure. Results are shown for two different grating pitches: (a) $p = 5$ μm and (b) $p = 20$ μm.

proximity of the distortion associated with these two boundaries. For a cell thickness of $d = 5$ μm the lower gradient at the boundary and the reduced value of twist $y = \pm 1.25$ μm significantly reduce the average twist angle in each domain. In Fig. 7(b), however, the pitch is $p = 20$ μm, so the regions at $y = \pm 1.25$ μm are close to only one domain boundary; thus the magnitude of the twist does not significantly reduce at these points and, more important, there is little effect in the bulk of the domain as the cell thickness increases.

Figure 8 shows the first-order diffraction efficiency η_1 as a function of the dimensionless parameter $\Delta nd/\lambda$ for pitch lengths p equal to 5, 10, and 20 μm and for y-polarized incident illumination. As before, each value of $\Delta nd/\lambda$ represents a different cell thickness and therefore a distinct 2D director profile. The curve for pitch $p = 20$ μm is very similar to that shown for the long-pitch limit in Fig. 5 but with the peak value of the diffraction efficiency reduced by 1.7%. This reduction indicates that the effect of the domain wall on η_1 is small for this pitch when the cell thickness is varying between d equal to 1 and 5 μm, i.e., $0 < \Delta nd/\lambda < 1.25$. For the pitch $p = 10$ μm there is a more marked reduction in the peak value of η_1 of 6.0%, and for the smallest pitch studied shown, $p = 5$ μm, the peak value of η_1 is reduced by 21.6% relative to the long-pitch limit. The reduction in the

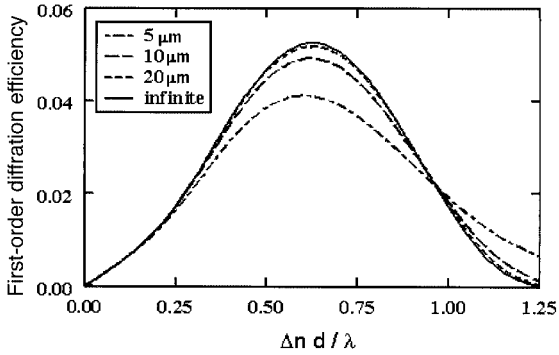

Fig. 8. First-order diffraction efficiency η_1 as a function of the parameter $\Delta nd/\lambda$ for the diffraction geometry in Fig. 2 with 2D elastic domain walls between the pixels as shown in Fig. 5. Results are shown for pitch lengths p of 5, 10, and 20 μm and for x-polarized incident illumination.

peak value of η_1 is accompanied by a shift to lower values of $\Delta nd/\lambda$ for the 5-μm pitch grating. In addition, at this pitch and for $\Delta nd/\lambda > 1$, the diffraction efficiency is significantly increased relative to the values given in the long-pitch limit.

In the simple model of a phase grating as an array of uniform birefringent slabs, the total diffraction efficiency is given by Eq. (1), which depends on the constant twist angles $\pm\beta$. These twist angles determine the difference in phase, i.e., the phase modulation, between neighboring pixels. For the nonuniform structures considered in this paper sophisticated VBPM methods have been needed to calculate η_1. However, the magnitude of the average twist angle in each domain still makes a major contribution in determining the magnitude of the diffraction efficiency η_1 for a given cell thickness, birefringence, and wavelength.

The results in Fig. 8 can be understood in terms of the reduction of the amount of phase modulation available from adjacent pixels due to the effect of the distortion associated with domain walls of finite width. Figure 6 showed an elastic domain wall, and Fig. 4 showed an artificially created abrupt boundary between two oppositely switched domains. The difference between the twist angles of the two domains is reduced in the region of the elastic domain wall relative to the case of an abrupt boundary. In this region, the amount of phase modulation possible between adjacent pixels is reduced, and so the diffraction efficiency is reduced accordingly.

For a SSFLC phase grating of pitch 20 μm a small fraction of the total phase-modulating volume is due to the distorted region adjacent to the domain boundary. Therefore the reduction of η_1 is small. This fraction is increased for the 10-μm pitch, but the most significant effect on η_1 occurs when the pitch is reduced further to 5 μm. For this grating pitch there is an additional reduction of the twist angle throughout the entire width of each of the domains, as shown in Fig. 7(b).

Figure 9 illustrates the polarization dependence of the first-order diffraction efficiency η_1 for pitch

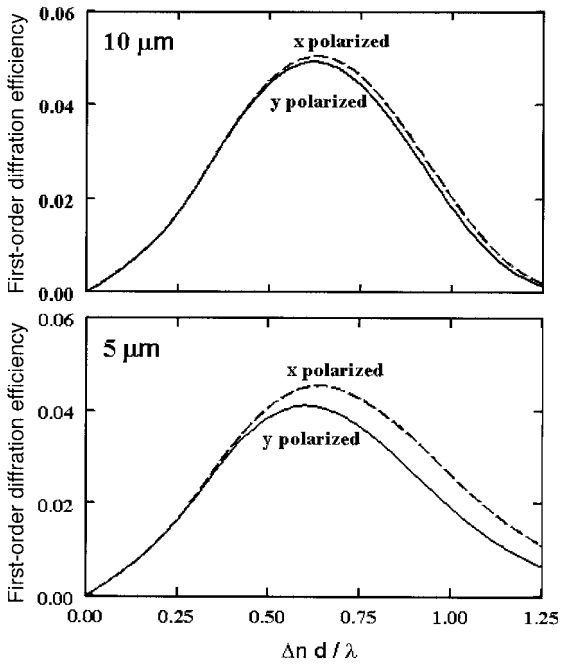

Fig. 9. Polarization dependence of the first-order diffraction efficiency η_1 shown in Fig. 8 for pitch lengths p of 5 and 10 μm.

lengths p equal to 5 and 10 μm. The variation of η_1 is shown as a function of the dimensionless parameter $\Delta nd/\lambda$ for pitch lengths $p = 10$ μm [Fig. 9(a)] and $p = 5$ μm [Fig. 9(b)], for both y- and x-polarized incident illumination. In each case the peak value of η_1 is changed for x-polarized light and shifted to higher values of $\Delta nd/\lambda$ relative to the curve for y-polarized light. The percent difference in the peak values are 11.3%, 2.4%, and 0.3% for pitches of 5, 10, and 20 μm (not illustrated), respectively. The dependence of η_1 on the polarization is therefore exacerbated at shorter pitches when a larger fraction of the SSFLC phase grating structure is influenced by the 2D elastic distortion at the domain boundaries.

5. Conclusions and Discussion

A LC continuum model has been used to describe the internal 2D structures in a phase grating consisting of alternating oppositely twisted domains in a SSFLC layer. The first-order diffraction efficiency η_1 for these structures has been calculated with a rigorous VBPM as a function of the layer thickness, the grating pitch, and the orientation of the polarization of incident light. As the grating pitch is reduced to 5 μm, it is found that the peak value of η_1 as a function of the parameter $\Delta nd/\lambda$ is significantly reduced relative to the ideal long-pitch limit and, furthermore, that the value of η_1 becomes dependent on the orientation of the polarization of the incident light. These observations can be attributed to the proportionally larger effects of the elastic domain walls on the propagation of the optical fields within the sample as the pitch is decreased.

We calculated the 2D director profiles in terms of the azimuthal angle, $\phi(y, z)$. It has been assumed that the LC director, which defines the local optical axis at a point within the layer, lies on a cone of fixed half-angle θ, which is tilted to the layer normal at a fixed layer tilt angle of either $+\delta$ or $-\delta$. Therefore, simple trigonometry can be used to convert the profile in $\phi(y, z)$ to the in-plane twist profile, $\beta(y, z)$. However, this geometry also leads to an out-of-plane tilt of the director,[16,28] which varies with position in the layer between 0° and 5°. Although this tilt variation is small and has been fully accounted for in the VBPM calculations presented here, there must be a line discontinuity in the tilt in the z direction at the domain boundaries. This discontinuity can be removed only with a more sophisticated LC theory that relaxes the condition that the cone angle θ is a constant quantity.[29–31]

The main assumption that has been made in the calculations of the internal structure of the SSFLC phase grating is that the orientation of the LC director at the chevron interface is fixed at one of two bistable orientations, $\phi(y, z = d/2) = \pm\phi_{ch}$ for the up domains or $\phi(y, z = d/2) = \pm(\pi - \phi_{ch})$ for the down domains. In theories that describe switching in one or two dimensions in SSFLC structures, often the chevron is implemented with a surface energy expression that has two minima corresponding to the two bistable positions,[32–34] for example, as exhibited by Eq. (4).

$$W = A\left[\left(\frac{\phi - \pi/2}{\phi_{ch}}\right)^2 - 1\right]^2 \tag{4}$$

This description would allow movement of the director at the chevron and would make the change in the twist ongoing from the up to the down domain at $z = d/2$ in Fig. 6 less abrupt. This reduced abruptness in turn could widen the region of elastic distortion occurring at the domain boundary. We have investigated the effects of using a chevron energy of the form given in Eq. (4) on the 2D director profiling using values of the parameter A down to 5.0×10^{-4} N m^{-1}. The foregoing is a typical value that allows experimental time–voltage switching curves in SSFLC devices to be reproduced.[35,36] We found an increase in the width of the elastic distortion region in the y direction, but this was not a highly significant effect. For the study of dynamic reorientation in devices with fixed boundary conditions, additional effects such as solitary wave switching may become important.[37]

The calculations we describe for the diffraction efficiencies have been performed with the appropriate material refractive indices for light at the red He–Ne laser wavelength of 633 nm and for transmission of light through the layer. A phase grating device that is destined for telecommunications applications would normally operate at a wavelength of either 1310 or 1550 nm. The device might also be fabricated with a reflective electrode structure on one surface of the SSFLC layer. One can make an estimation of the variation of the diffraction efficiency with pitch, cell thickness, and input polarization for

these different wavelengths and for the case of a reflective geometry by a simple scaling of the value of the parameter $\Delta nd/\lambda$ on the horizontal axis of the graphs we have presented. For accurate results, however, the full VBPM results would need to be repeated and with values of refractive index that are appropriate for the wavelength used.

References

1. R. M. Turner, D. A. Jared, G. D. Sharp, and K. M. Johnson, "Optical correlator using very-large-scale integrated/circuit ferroelectric-liquid-crystal electrically addressed spatial light modulators," Appl. Opt. **32,** 3094–3101 (1993).
2. T. D. Wilkinson, Y. Petillot, R. J. Mears, and J. L. de Bougrenet de la Tocnaye, "Scale-invariant optical correlators using ferroelectric liquid-crystal spatial light modulators," Appl. Opt. **34,** 1885–1890 (1995).
3. S. E. Broomfield, M. A. Neil, and E. G. S. Paige, "Programmable multiple-level phase modulation that uses ferroelectric liquid-crystal spatial light modulators," Appl. Opt. **34,** 6652–6665 (1995).
4. R. J. Mears, W. A. Crossland, M. P. Dames, J. R. Collington, M. C. Parker, S. T. Warr, T. D. Wilkinson, and A. B. Davey, "Telecommunications applications of ferroelectric liquid-crystal smart pixels," IEEE J. Sel. Topics Quantum Electron. **2,** 35–46 (1996).
5. W. A. Crossland, I. G. Manolis, M. M. Redmond, K. L. Tan, T. D. Wilkinson, M. J. Holmes, T. R. Parker, H. H. Chu, J. Croucher, V. A. Handerek, S. T. Warr, B. Robertson, I. G. Bonas, R. Franklin, C. Stace, H. J. White, R. A. Woolley, and G. Henshal, "Holographic switching: the ROSES demonstrator," J. Lightwave Technol. **18,** 1845–1854 (2000).
6. N. A. Clark and S. T. Lagerwall, "Sub-millisecond bistable electro-optic switching in liquid crystals," Appl. Phys. Lett. **36,** 899–901 (1980).
7. J. C. Jones, M. J. Towler, and J. R. Hughes, "Fast, high contrast ferroelectric liquid crystal displays and the role of dielectric biaxiality," Displays **14,** 86–93 (1993).
8. S. E. Broomfield, M. A. Neil, E. G. Paige, and G. G. Yang, "Programmable binary phase-only device based on ferroelectric liquid crystal SLM," Electron. Lett. **28,** 26–28 (1992).
9. C. W. Slinger, R. W. Bannister, C. D. Cameron, S. D. Coomber, I. Cresswell, P. M. Hallett, J. R. Hughes, V. C. Hui, J. C. Jones, R. Miller, V. Minter, D. A. Pain, D. C. Scattergood, D. T. Sheerin, M. J. Smith, and M. Stanley, "Progress and prospects for practical electro-holographic display systems," in *Practical Holography XV and Holographic Materials VII*, S. A. Benton, S. H. Sylvia, and T. J. Trout, eds., Proc. SPIE **4296,** 18–32 (2001).
10. See, for example, J. Senior, *Optical Fiber Communications: Principles and Practice*, 2nd ed. (Prentice Hall, N.J., 1992).
11. S. Warr and R. Mears, "Polarization-insensitive operation of ferroelectric liquid crystal devices," Electron. Lett. **31,** 714–716 (1995).
12. S. Warr and R. Mears, "Polarisation insensitive diffractive FLC systems," Ferroelectrics **181,** 53–59 (1996).
13. See, for example, J. W. Goodman, *Introduction to Fourier Optics* (McGraw-Hill, N.Y., 1996).
14. N. A. Clark and T. P. Reiker, "Smectic C chevron, a planar liquid-crystal defect-implications for the surface stabilized ferroelectric liquid crystal geometry," Phys. Rev. A **37,** 1053–1056 (1988).
15. M. H. Anderson, J. C. Jones, E. P. Raynes, and M. J. Towler, "Optical studies of thin layers of smectic C materials," J. Phys. D: Appl. Phys. **24,** 338–342 (1991).
16. C. V. Brown and E. E. Kriezis, "Calculation of the efficiency of polarization-insensitive surface-stabilized ferroelectric liquid-crystal diffraction gratings," Appl. Opt. **42,** 2257–2263 (2003).
17. J. Z. Xue and N. A. Clark, "Stroboscopic microscopy of ferroelectric liquid crystals," Phys. Rev. E **48,** 2043–2054 (1993).
18. T. Carlsson, I. W. Stewart, and F. M. Leslie, "An elastic energy for the ferroelectric chiral smectic C* phase," J. Phys. A **25,** 2371–2374 (1992).
19. C. V. Brown and J. C. Jones, "Accurate determination of the temperature and frequency dependent smectic C biaxial permittivity tensor," J. Appl. Phys. **86,** 3333–3341 (1999).
20. E. E. Kriezis and S. J. Elston, "Wide-angle beam propagation method for liquid-crystal device calculations," Appl. Opt. **39,** 5707–5714 (2000).
21. E. E. Kriezis and S. J. Elston, "Light propagation in liquid crystal displays by the 2-D finite-difference time-domain method," Opt. Commun. **177,** 69–77 (2000).
22. B. Wang, P. J. Bos, and C. D. Hoke, "Light propagation in variable-refractive-index materials with liquid-crystal-infiltrated microcavities," J. Opt. Soc. Am. A **20,** 2123–2130 (2003).
23. M. J. Towler, J. R. Hughes, and F. C. Saunders, "Switching behaviour of smectic C* liquid crystals," Ferroelectrics **113,** 453–465 (1991).
24. J. Chen, P. J. Bos, H. Vithana, and D. L. Johnson, "An electro-optically controlled liquid crystal diffraction grating," Appl. Phys. Lett. **67,** 2588–2590 (1995).
25. C. M. Titus and P. J. Bos, "Efficient, polarisation-independent, reflective liquid crystal phase grating," Appl. Phys. Lett. **71,** 2239–2241 (1997).
26. Z. He and S. Sato, "Polarization properties of inversely twisted nematic liquid-crystal gratings," Appl. Opt. **37,** 6755–6763 (1998).
27. See, for example, M. Boas, *Mathematical Methods in the Physical Sciences* (Wiley, New York, 1983).
28. E. E. Kriezis, S. K. Filippov, and S. J. Elston, "Light propagation in domain walls in ferroelectric liquid crystal devices by the finite-difference time-domain method," J. Opt. A Pure Appl. Opt. **2,** 27–33 (2000).
29. M. Nakagawa, "Theoretical study of the chevron layer structure in smectic phases," Displays **11,** 67–72 (1990).
30. N. Vaupotič, S. Kralj, M. Čopič, and T. J. Sluckin, "Landau-de Gennes theory of the chevron structure in a smectic liquid crystal," Phys. Rev. E **54,** 3783–3792 (1996).
31. N. Vaupotič and M. Čopič, "Structure and energy of the wall separating two states in surface-stabilized smectic C chevron cells," Liq. Cryst. **26,** 1429–1435 (1999).
32. J. E. Maclennan, M. A. Handschy, and N. A. Clark, "Director reorientation dynamics in chevron ferroelectric liquid crystal cells," Liq. Cryst. **7,** 787–796 (1990).
33. M. J. Towler, J. C. Jones, and E. P. Raynes, "The effect of the biaxial permittivity tensor and tilted layer geometries on the switching of ferroelectric liquid crystals," Liq. Cryst. **11,** 365–371 (1992).
34. P. Maltese, R. Piccolo, and V. Ferrara, "An addressing effective computer model for surface stabilized ferroelectric liquid crystal cells," Liq. Cryst. **15,** 819–834 (1993).
35. J. C. Jones, C. V. Brown, and P. E. Dunn, "The physics of tVmin ferroelectric liquid crystal displays," Ferroelectrics **246,** 1097–1107 (2000).
36. S. M. Said and S. J. Elston, "Modelling of switching in surface-stabilised ferroelectric liquid crystal cells using a three-variable model in one dimension," Liq. Cryst. **28,** 561–571 (2001).
37. I. Abdulhalim, G. Moddel, and N. A. Clark, "Director–polarization reorientation via solitary waves in ferroelectric liquid crystals," Appl. Phys. Lett. **60,** 551–552 (1992).